

The BiomolBiomed publishes an "Advanced Online" manuscript format as a free service to authors in order to expedite the dissemination of scientific findings to the research community as soon as possible after acceptance following peer review and corresponding modification (where appropriate). An "Advanced Online" manuscript is published online prior to copyediting, formatting for publication and author proofreading, but is nonetheless fully citable through its Digital Object Identifier (doi®). Nevertheless, this "Advanced Online" version is NOT the final version of the manuscript. When the final version of this paper is published within a definitive issue of the journal with copyediting, full pagination, etc., the new final version will be accessible through the same doi and this "Advanced Online" version of the paper will disappear.

RESEARCH ARTICLE

Jebahi et al: Plant-based ZnO nanoparticles study

Green synthesis of plant-derived ZnO nanoparticles: Characterization, pharmacokinetics, molecular interactions, and *in-vitro* antimicrobial and antifungal evaluation

Samira Jebahi^{1,2}, Riadh Badraoui^{3,4*}, Ghada Ben Salah⁵, Fadia Ben Taheur⁶, Faten Brahmi⁷, Mohsen Mhadhbi⁸, Talel Bouhamda⁹, Saoussen Jilani³, Bandar Aloufi³, Mohd Adnan³, Arif J. Siddiqui³, Abdel Moneim E. Sulieman³, Ines Karmous^{1,10}

¹Biology and Environmental department, Insitute of Applied Biology of Medenine (ISBAM), University of Gabes, Medenine, Tunisia.

²Research Laboratory on Energy and Matter for Nuclear Sciences Development (LR16CNSTN02), National Center for Nuclear Sciences and Technologies, Sidi Thabet Technopark 2020 Ariana, Tunisia

³Department of Biology, College of Science, University of Ha'il, Ha'il, Saudi Arabia

⁴Section of Histology-Cytology, Medicine Faculty of Tunis, University of Tunis El Manar, La Rabta-Tunis, Tunisia

⁵Department of Pharmacology and Toxicology, College of Pharmacy, Qassim University, Al Qassim, Saudi Arabia.

⁶Laboratory of Analysis, Treatment and Valorization of Environmental Pollutants and Products, Faculty of Pharmacy, University of Monastir, Rue Ibn Sina, Monastir, Tunisia.

⁷Department of Chemistry, College of Science, University of Ha'il, Ha'il, Saudi Arabia.

⁸Laboratory of Useful Materials, National Institute of Research and Physicochemical Analysis, Technopole Sidi Thabet, Ariana, Tunisia

⁹Arid Land Region Institute of Medenine (IRA), Medenine, Tunisia.

¹⁰Plant Toxicology and Molecular Biology of Microorganisms, Faculty of Sciences of Bizerte, Zarzouna, Tunisia.

*Correspondence to Riadh Badraoui: riadh.badraoui@fmt.utm.tn; badraouir@yahoo.fr

DOI: <https://doi.org/10.17305/bb.2025.12090>

ABSTRACT

Nowadays, nanoparticles (NPs) are used to counteract various medicinal and industrial problems. This study aimed to biosynthesize zinc oxide NPs (ZnONPs) from the plant species *Aloe vera* L., *Peganum harmala* L., *Retama monosperma* L., and *Thymelaea hirsuta* L. The biosynthesized ZnONPs were referred to as “Thymhirs.bio-ZnONP,” “Aloever.bio-ZnONP,” “Retam.bio-ZnONP,” and “Harm.bio-ZnONP.” A UV-visible spectrophotometer, granulometry, Fourier transform infrared spectroscopy, and electron paramagnetic resonance were used for physicochemical characterization. Pharmacokinetics and antimicrobial effects were explored using combined *in vitro* and computational assays. An abundance of phenolic acids and flavonoids was observed, particularly rutin, quinic acid, apigenin-7-O-glucoside,

and cirsiol, which may act as reducing, stabilizing, and capping agents in the biosynthesis. ZnONPs demonstrated strong antimicrobial activity against various bacterial, fungal, and yeast strains, highlighting their potential medicinal applications. This inhibitory activity can be attributed to the effect of the plant-based ZnO nanosized particles more than to the plant extracts or Zn salt. Computational modeling revealed that the identified phytochemicals (phenolic acids and flavonoids) bound Tyrosyl-tRNA Synthetase (TyrRS) from *S. aureus* (1JJJ), aspartic proteinase from *C. albicans* (2QZW), and wheat germ agglutinin (2UVO) with considerable affinities, which, together with molecular interactions and pharmacokinetics, satisfactorily support the *in vitro* antimicrobial findings. This study lays the groundwork for future research and pharmaceutical explorations aimed at harnessing the likely beneficial properties of green-synthesized ZnONPs for medicinal and therapeutic purposes, particularly their antimicrobial effects.

Keywords: Antibacterial and antifungal activities, biosynthesis, nanotechnology, phytochemicals, zinc oxide nanoparticles, ZnONPs, computational modeling.

INTRODUCTION

The engineering of nanoparticles (NPs) has become an extensive concern due to their potential application in various domains in science and technology [1, 2]. NPs are nanomaterials with nano-sized range of 10–100 nm, and a larger surface area by volume ratio than the bulk materials. Manufacturing NPs involves chemical and physical methods, which are usually time-consuming, costly, and toxic. Therefore, the green synthesis of NPs has been developed as a fast, cheap, and eco-friendly alternative [3]. In addition, the biosynthetic routes provide better-defined sizes and morphology for NPs, as compared with other physicochemical methods [4]. The green synthesis of metal and metal oxide NPs involves either plants and their derivatives, or microorganisms, such as bacteria, fungi, algae and yeast [5–7]. Among plant species that were used in the biosynthesis of zinc oxide nanoparticles (ZnONPs), *Sageretia thea* [8] *Zingiber officinale* [9], *Catharanthus roseus* [10], *Laurus nobilis* L. [11], *Cannabis sativa* [12], *Ceratonia siliqua* [13] and *Artemisia vulgaris* [14].

In general, ZnONPs have been incorporated in medicinal purposes, including drug delivery, antimicrobial and antioxidant activities, as well as diagnosis of diseases [15, 16]. Besides, biologically synthesized NPs have shown efficiency as antimicrobial agents, drug carriers, and fillings in medical materials [17, 18].

To the best of knowledge, this is the first-time study that focuses on the green synthesis of ZnONPs, using the plant species *Thymelaea hirsuta* L., *Aloe vera* L., *Retama monosperma* L., and *Peganum harmala* L. These plants usually grow in harsh desert environments, and have medicinal applications. *Thymelaea hirsuta* L. (common name: Mitnan) is a perennial, evergreen and desert shrub, which belongs to the plant family of Thymelaeaceae, and grows up to 2 m tall. *T. hirsuta* L. grows in the Mediterranean coastal plains, the Sinai Peninsula and Saharo-Arabian deserts. Interesting medicinal properties have been attributed to *T. hirsuta* L., such as being an antidote to pinworms, an anti-inflammatory agent, and a powerful cathartic, hydragogue, and expectorant. Other medicinal uses of *T. hirsuta* L. include improving healing, and being a remedy in cases of carious teeth, eye diseases, and paralysis. Also, *T. hirsuta* L. played an inhibiting role of the progression of hepatocellular carcinoma [19]. *Aloe vera*, is a succulent plant that belongs to the genus *Aloe*. It is an evergreen wild perennial that grows in arid, tropical, and semi-tropical climates. The leaves of *A. vera* contain promising phytochemicals, such as acetylated mannans, polymannans, anthraquinone C-glycosides, anthrones, emodin and lectins [20]. These bioactive components attribute to *A. vera*'s beneficial roles, such as antioxidant, health-promoting, anti-inflammatory, and nutritional effects. Indeed, it is widely used in cosmetic, and in pharmaceutical and food industry. Several health benefits have been reported for *A. vera* include its efficiency in wound healing, treating burns, protecting skin from X-rays, also against lung cancer, intestinal problems, diabetics, allergies, and acquired immune deficiency syndrome. *Peganum harmala* L., also known as wild rue or harmel, is a perennial and herbaceous plant that belongs to the family Nitrariaceae. It is usually grown in saline soils in temperate desert and Mediterranean regions [21], and is considered a noxious weed and invasive species in some regions of the western United States. *P. harmala* has been useful in ethnopharmacology as a remedy for many health problems, such as fever, diarrhea, body pains, abortion, and subcutaneous tumors [21]. Among the important bioactivities of *P. Harmala*, its anticholinesterase, anti-cancer, anti-inflammatory, antioxidant, antiparasitic, and antibacterial effects [22, 23]. This plant is rich in β -carboline alkaloids, such as harmine, harmaline, harmalol, harman and quinazoline derivatives, which are responsible of *P. harmala* L. toxicity to domestic animals and humans [21].

Overall, the plant species described above are either aromatic, ornamental and medicinal, or considered as invasive species that could be sometimes injurious to agricultural and horticultural crops, ecosystems, and humans. In the current study, we aimed to use the extracts of these plants as reducing agents in the synthesis of ZnONPs. A special interest was

mainly attributed to the investigation of the antimicrobial activity against some bacterial and fungal microorganisms, including *S. aureus*, *M. luteus*, *C. albicans* and *A. flavus*. Furthermore, bioavailability, pharmacokinetic properties of the phenolic acids and flavonoids, which have been identified by HPLC-MS extracts of *Thymelaea hirsuta* L., *Aloe vera* L., *Retama monosperma* L. and *Peganum harmala* L. and their molecular interactions with some key receptors were studied by computational modeling.

MATERIALS AND METHODS

Biosynthesis of zinc oxide nanoparticles

Plants of *Thymelaea hirsuta* L., *Aloe vera* L., *Retama monosperma* L., and *Peganum harmala* L. were collected from the region “Beni Kdech” and “Bir Lahmar” in the state of Medenine in Tunisia (in March 2020). Dr. Samir Tlahig (Specialist in Botany) identified the plant species, using the botanical guide of “La flore de la Tunisie, Med-checklist”, and the online databases of Plants of the World Online (POWO). The aerial parts (leaves and shoots) of plants were air-dried for 5 days (at approximate temperature of 30-35°C). Dry leaves (5 g) were ground using mortar to obtain a powder, and homogenized in 50 mL of distilled water (1:10, w/v). Homogenates were filtered using ash free filter papers, and stored at 4°C. A volume of plant homogenates was mixed with 0.1 M zinc acetate dehydrates. The mixture was allowed to incubate in boiling water for 2 h at 80°C. The precipitate of zinc oxide nanoparticles (ZnONPs) was collected as the pellet resulting from the centrifugation of the mixture for 10 min at 8000 ×g. The supernatants were thrown, and the pellets were washed three times with distilled water to get rid of impurities. The obtained ZnONPs were referred by “*Thymhirs.bio-ZnONP*” for *Thymelaea hirsuta* L. based ZnONP, and “*Aloever.bio-ZnONP*” for *Aloe vera* L. based ZnONP, “*Retam.bio-ZnONP*” for *Retama monosperma* L. and “*harm.bio-ZnONP*” for *Peganum harmala* L.

Biophysical characterization

The structural properties of biologically synthesized ZnONPs were characterized using a UV-vis spectrophotometer [14]. Based on granulometry, the distribution of particle size and the surface area were determined using a laser analyzer Malvern Master-sizer 2000 in the range of 0.02 to 2000 μm. A Bruker Equinox 55 spectrometer at wavelength range of 400-4000 cm⁻¹, was used to obtain Fourier Transform Infra-Red spectra (FTIR) to identify the functional groups and phytochemicals at the surface of ZnONPs. The electron paramagnetic resonance (EPR) spectrum was recorded using a Bruker ER-200D spectrometer, operating at

9.8 GHz X-Band frequencies with modulation amplitude of 0.2 mT, modulation frequency of 100 kHz sweep width of 210 mT and microwave power of 63 mW. Data were acquired at a power of 2 mW with a spectral width of 3200-3800 Gauss.

Analysis of the flavonoids and phenolic compounds by liquid chromatography coupled to mass spectrometry (HPLC-MS)

The phenolic compounds were extracted by the homogenization of dry leaves in 80% methanol (1:10, w/v), followed by centrifugation at $10,000 \times g$ for 20 min. Supernatants were then filtered through a $0.45 \mu\text{m}$ cellulose acetate filter (Millipore), and a volume of $20 \mu\text{L}$ was loaded on a CTO-20 AC column for analysis by Liquid Chromatography coupled to Mass Spectrometry (HPLC-MS, Shimadzu UFLC XR system, Kyoto, Japan). The system includes a LC-20ADXR binary pump and a quadrupled 2020 detector, an inertial ODS-4 C18 $3 \mu\text{m}$ column $\text{L}150 \times 3.0 \text{ mm}$, set at 40°C . The conditions of the run consist of a flow rate of 0.5 mL min^{-1} , a mobile phase composed of solution A [5% methanol, 0.15% acetic acid] and solution B [50% ACN, 0.15% acetic acid]. Both washes and equilibration of the column were done using 10% of solution B for 45-50 min. Conditions consisted of 275°C dissolving line temperature, 1.50 mL min^{-1} mobilizing gas flow, $15.00 \text{ mL min}^{-1}$ drying gas, and 450°C temperature of heat block. Elution was performed in a linear gradient using solution B, as following; 10-20% for 0.01-14 min, 20-55% for 14-27 min, 55-100% for 27-37 min, and 100% for 37-45 min. LC-ESI-MS mass spectra [M-H]⁻ were acquired using lab solutions software. The identification and quantification of phenolic acids were done with reference to the mass-spectrum of the lab standards of polyphenolic compounds (LGC and Sigma Aldrich).

Assay of the antibacterial activity

The bacterial strains used were: two strains of Gram positive (*Staphylococcus aureus* (ATCC 25923) and *Micrococcus luteus* (NCIMB8166) and two strains of Gram negative (*Salmonella enterica* serotype Typhimurium (ATCC1408) and *Escherichia coli* ATCC35218). The culture of the bacterial strains was carried out on a nutritive agar, at 37°C for 24 h. Selected colonies were inoculated into a 10 mL suspension of sterile physiologic water, and mixed for 5 min. Bacterial growth was monitored by measuring the optic density (OD) of the culture at 600 nm, and adjusted up to the absorbance value of 0.5. A volume of 1 mL of the bacterial culture was spread on Muller Hinton agar. Then, a volume of $100 \mu\text{L}$ (corresponding to a concentration of $10 \times 10^3 \text{ ppm}$) of ZnONPs (corresponding to a quantity of 0.1 mg) was added

into wells of 6 mm diameter. Bacteria was incubated at 37°C for 24 h, and then the diameter of inhibition zone (mm) was measured using digital caliper. The antibacterial assays were carried out in triplicates and , and under sterile conditions. Control assays were carried using plant extracts of *Thymelaea hirsuta L.*, *Aloe vera L.*, *Retama monosperma L.*, and *Peganum harmala L.*, Zinc acetate salt, and 10 µg/mL Gentamicin.

Activity against yeast growth

Yeast strains consisted of *Candida albicans* (ATCC90028), *Candida krusei* (ATCC6258) and *Candida neoformans* (ATCC14116). Culture was performed on Sabouraud agar, at 37°C for 48 h. Selected colonies were used for yeast culture in suspension. Growth was monitored by measuring the OD of the culture at 600 nm, and adjusted up to OD value 0.5. One mL of suspension of yeast was inoculated on Sabouraud agar plates, then incubated at 37°C for 30 min. A volume of 100 µL (corresponding to a concentration of 10×10^3 ppm of ZnONPs) (corresponding to a quantity of 0.1 mg) was added into wells of 6 mm diameter on agar. After incubation for growth at 37°C for 48 h, the diameter of inhibition zone was measured and expressed in mm. The experimental antifungal assays were carried out in triplicates, and under sterile conditions. Control assays were carried using plant extracts of *Thymelaea hirsuta L.*, *Aloe vera L.*, *Retama monosperma L.*, and *Peganum harmala L.*, Zinc acetate salt, and 10 µg/mL Cycloheximide.

Assay of the antifungal activity

Fungal strains, *Aspergillus flavus* (15UA005), *Aspergillus niger* (15UA006) and *Aspergillus fumigatus* (ATCC204305) were cultured on Sabouraud agar at 25°C for 7 days. Spores of each fungal strain were, separately, transferred into a suspension of peptone water, and counted up to 10⁶ spores/mL. A volume of 1 mL of fungal suspension was inoculated on Sabouraud agar, and incubated for growth at 25 °C for 30 min. Then, a volume of 100 µL (corresponding to 10×10^3 ppm of each ZnONP) (corresponding to a quantity of 0.1 mg) was added into 6 mm-diameter wells. Following incubation for yeast growth at 25 °C for 48 h, the diameter of inhibition zone was measured, and expressed in mm. The experimental antifungal assays were carried out in triplicates, and under sterile conditions. Control assays were carried using plant extracts of *Thymelaea hirsuta L.*, *Aloe vera L.*, *Retama monosperma L.*, and *Peganum harmala L.*, Zinc acetate salt, and 10 µg/mL Cycloheximide.

Computational modeling assay and interactions analyses

The phytochemicals of the phenolic acids and flavonoids, which have been identified on *Thymelaea hirsuta* L., *Aloe vera* L., *Retama monosperma* L. and *Peganum harmala* L. were used for the computational modeling to explore their molecular interactions with some key receptors (Tyrosyl-tRNA Synthetase (TyrRS), secreted aspartic proteinase, and wheat germ agglutinin) involved in the antimicrobial effects. Hence, the 3D structure of these phytochemicals was collected from the pubchem website or drawn using ChemDraw Pro 12.0 software package. The 3D crystal structure of TyrRS from *S. aureus* (Tyrosyl-tRNA Synthetase (TyrRS) (protein data bank, pdb ID: 1JIJ), the secreted aspartic proteinase 1 from *C. albicans* (pdb ID: 2QZW), and wheat germ agglutinin (pdb ID: 2UVO) receptors was collected from the RCSB PDB. The collected receptors and ligands were prepared by removing water molecules, adding polar hydrogen and Kollman charges, then processed for minimization as previously reported [24–26]. Both complex subunits (receptors and ligands) were subjected to force field of CHARM force field after the the determination of the grid box using vina software packages [25, 27, 28].

Bioavailability and pharmacokinetics

Both bioavailability and pharmacokinetics of the phenolic acids and flavonoids, which have been identified on *Thymelaea hirsuta* L., *Aloe vera* L., *Retama monosperma* L. and *Peganum harmala* L. have also been studied as previously reported [27, 29]. The computational assessment of these parameters was based on the ADMET (for absorption, distribution, metabolism, excretion and toxicity) measurements [28, 30], and calculation of flexibility (flex), insaturation (insatu), insolubility (insolu), lipophilicity (lipo), molecular size (size), and polarity (pola) of the compounds using SwissADME.

Statistical analysisThe statistical analyses were performed using SPSS (version 20). The provided data represent mean±SD. Comparisons between types of nanoparticles were performed using ANOVA at $\alpha=0.05\%$, followed by Post Hoc test of Duncan multi-range test at 5%.

RESULTS

Chemical and physical properties of nascent zinc oxide nanoparticles

Thymelaea hirsuta L., *Aloe vera* L., *Retama monosperma* L., and *Peganum harmala* L. were used to biosynthesize bio-ZnONPs namely *Thymhirs.bio-ZnONP*, *Aloever.bio-ZnONP*, *Retam.bio-ZnONP*, and *harm.bio-ZnONP*, respectively. The nascent bio-ZnONPs were confirmed by the measurement of the UV-vis absorption spectrum, showing typical absorption peaks at 340-360 nm (Figure 1).

Concerning the size distribution of ZnONPs (Figure 2), *Thymhirs.bio-ZnONP* showed an average size of 392 nm at d 0.1, and 543 nm at d 0.5; *Aloever.bio-ZnONP* showed an average size of 410 nm at d 0.1, and 742 nm at d 0.5; *Retam.bio-ZnONP* showed an average size of 742 nm at d 0.1, and 980 nm at d 0.5; while *harm. bio-ZnONP* showed an average size of 255 nm at d 0.1 and 348 nm at d 0.5 (Table 1). FTIR analysis revealed peaks which occurred at 1634 and (600, 450) cm^{-1} corresponded, respectively to Zn–O stretching and the deformation vibration, respectively. The absorption peaks of metal oxides usually occurred in the regions between 600 and 400 cm^{-1} . The broad peak seen at about 3300 cm^{-1} exhibits the OH stretching vibrations.

FTIR spectra of *Thymhirs.bio-ZnONP* (Figure 3) showed a band at 2950-2850 cm^{-1} . This peak corresponded to stretching of C-H of alkane compounds. In the FTIR spectra, the absorption peak at 2350 cm^{-1} implies the stretching of O=C=O of carbon dioxide. The absorption peak at 1450 cm^{-1} may correspond to O–H bending of carboxylic acid. The stretching vibrations which were situated at 1050 cm^{-1} and 850 cm^{-1} correspond to CO-O-CO stretching of anhydride and C-H bending, respectively. *Aloever.bio-ZnONP* showed absorption peaks at 3250-3400 cm^{-1} corresponding to OH stretching of alcohol, and at 1600 cm^{-1} of C=C stretching of α , β unsaturated ketone. *Retam.bio-ZnONP* also showed a broad peak at 3250 cm^{-1} corresponding to O-H groups that can be attributed to either phenols or carboxylic acid, and a peak at 1600 cm^{-1} of C=C stretching of α , β unsaturated ketone. These functional groups like –C–H and –C=C may be involved in as capping agents of ZnONPs, allowing to stabilize ZnONPs to prevent further growth and agglomeration.

HPLC-MS results of phenolic acids and flavonoids

The phenolic acids and flavonoids of the used plants extracts were evaluated by HPLC-MS (Table 2). Obtained results revealed several phenolic compounds that may potentially act as reducing, stabilizing and capping agents during the biosynthesis of ZnONPs. *P. harmala*.

showed the highest levels of quinic acid, gallic acid, transferulic acid, rutin, luteolin-7-o-glucoside, 3,4-di-O-caffeoyquinic acid, caffeic acid and naringenin. Other compounds were species dependent, such as in *T. hirsute*; quercetin, in *A. vera*; Protocatechuic acid, Quercetin (quercetin-3-o-rhamonosic), Rosmarinic acid, catechin and epicatechin. Also, *A. vera* showed the highest levels of phenolic compounds, notably rutin, caffeic acid, salviolinic acid, Hyperoside(quercetin-3-o-galactoside), Apegenin-7-o-glucoside, trans cinnamic, Chlorogenic acid, syringic acid and cirsiolol. In regard to *R. monosperma* L., it mainly contains quinic acid, rutin, 3,4-di-O-and caffeoyquinic acid (Table 2).

The electron paramagnetic resonance (EPR) spectra (Figure 4) showed no magnetic properties for “*Thymhirs.bio-ZnONP*”, while clearly visible paramagnetic properties were detected for “*Aloever.bio-ZnONP*” and “*Retam.bio-ZnONP*”. In EPR spectrum, signal intensity reflected the total absorbed energy of bio-ZnONPs under resonance, and showed that EPR spectrum exhibited a distinct paramagnetic signal at $g=2.0124$ which is attributed to V_O-V_{Zn} clusters.

Biological activities

Table 3 exhibits the obtained bio-ZnONPs were analyzed for their potential activity against various microbes, including the growth of bacteria, yeast and fungi (Table 3). Disk diffusion is a qualitative or semi-quantitative method, and its sensitivity depends on multiple factors including the compound's diffusion rate through the agar, its concentration, and the microbial susceptibility. A zero inhibition zone in antimicrobial assays in disk diffusion methods, does not necessarily confirm the complete absence of antimicrobial activity. Rather, it suggests that if there is any effect, it's below the detection limit of the assay that we used in our experiment. We considered the inhibition zones with diameters of 15 mm or more indicative of a strong antimicrobial activity; the inhibition zones ranging from 10 mm to 14 mm for a moderate antimicrobial activity; and the inhibition zones with diameters less than 10 mm indicating a weak antimicrobial activity. The highest antibacterial activity was recorded against *Staphylococcus aureus* ATCC 25 923 for *Thymhirs.bio-ZnONP* with inhibition zone of 15 ± 1.41 mm, and against *Micrococcus luteus* NCIMB 8166 for *Aloever.bio-ZnONP* inhibition zone of 24 ± 0.00 mm. *Retam.bio-ZnONP* also exhibited an inhibiting activity against *S. aureus* (with inhibition zone 11 ± 0.71 mm), *M. luteus* (with inhibition zone 13 ± 0.71 mm) and *S. enterica serotype Typhimurium* (with inhibition zone 11 ± 0.00 mm). *harm.bioZnONP* also inhibited the growth of *S. aureus* (13 ± 0.71 mm) and *M. luteus* (12 ± 0.71

mm), versus no effect against *S. enterica* and *E. coli*. In addition, *Thymhirs*.bio-ZnONP showed inhibiting activity against only one yeast strain (Table 3); *Candida albicans* ATCC90028. However, *Aloever*.bio-ZnONP exhibited an inhibitory activity on the growth of three tested yeast strains; *C. albicans*, *C. krusei* and *C. neoformans*, respectively, with inhibition zones of 14 ± 0.71 mm, 12 ± 0.71 mm, and 11 ± 0.00 mm. *Retam*.bio-ZnONP also had an inhibitory activity against *C. albicans* with inhibition zone 13 ± 0.00 , while *harm*.bioZnONP could inhibit only *C. neoformans* by 16 ± 0.71 (Table 3). This limited inhibitory activity of *harm*.bioZnONP was, however, different when *harm*.bioZnONP were tested against fungal growth. Interestingly, a significant inhibitory activity of *harm*.bioZnONP was found against all *Aspergillus* species, with an increasing inhibition order; *A. flavus*<*A. niger*<*A. fumigatus*. Similarly, inhibitory activities of *Thymhirs*.bio-ZnONP were detected against *Aspergillus flavus* and *Aspergillus fumigatus*, for which the inhibition zones reached 16 ± 0.71 mm and 12 ± 0.00 mm, respectively. *Aloever*.bio-ZnONP also showed an antifungal activity against all strains of *Aspergillus*, and the highest ones were recorded against *A. flavus* and *A. fumigatus*. *Retam*.bio-ZnONP also inhibited the growth of *A. flavus* by 17 ± 0.71 mm (Table 3).

We also compared our findings with the effects of the plants extracts respective to ZnONPs (Table 3). Our results revealed no detectable (0 mm) or weak (inhibitory diameter < 10 mm antibacterial activity for most of the plant species, except a strong activity ($15\pm 1,00$ mm), while moderate inhibition of all bacterial, yeast and fungal strains was observed by *Peganum harmala*(Table 3). This antimicrobial activity was similarly found weaker (<10 mm) with Zn acetate salt against all microbial strains tested (Table 4), except a moderate inhibitory activity against *Staphylococcus aureus* and *Micrococcus luteus* (Table 4).

Computational findings: pharmacokinetics and molecular interactions

Lipophilicity, druglikeness and pharmacokinetic properties of the phenolic acids and flavonoids of *Thymelaea hirsuta* L., *Aloe vera* L., *Retama monosperma* L. and *Peganum harmala*. L. are shown in Table 5. The majority of these phytochemicals meet the Lipinski rule and have acceptable druglikeness properties. Based on flexibility (flex), insaturation (insatu), insolubility (insolu), lipophilicity (lipo), molecular size (size), and polarity (pola), the studied compounds possessed acceptable oral bioavailability scores varying from 0.11 to 0.85. This supported their potential bioactivities. Both blood-brain-barrier (BBB) permeation and gastro-intestinal (GI) absorption have been explored and used for designing of the egg-

model (Figure 5). Most of identified phytochemicals are not substrate of P-glycoprotein (P-gp) substrates and have acceptable skin permeation as Log K_p ranged between -5.66 and -9.15. Table 4 exhibited that while each of these studied CYPs was inhibited by only few compounds, CYP2C19 was not inhibited by any of the phytochemicals. The synthetic accessibility was found to range between 1.07 and 5.28.

It was predicted that all these phytochemicals had negative but varied binding affinities to each of 1JJJ, 2QZW and 2UVO receptors (Table 6). These affinities reached -10.5, -10.0 and -8.4 kcal/mol for 1JJJ, 2QZW and 2UVO, respectively. These best binding affinities concerned the phytochemicals no. 12, 8 and 16 respectively (Tables 6 and 7). Many identified phytochemicals were predicted to established good molecular interactions with each of the studied receptors and included up to 9 conventional H-bonds. For instance, compound no. 8 established 9 conventional H-bonds, which have been supported with van der Waals and Pi-alkyl bonds (Figure 6). These interactions concerned LYS49, SER89, ASN160, LYS178, SER336, GLY87, PRO4, ILE338, and THR166. The latter was complexed with the compound no. 8 via 3 conventional H-bonds and was the closest interacting residue (2.150 Å).

DISCUSSION

The biosynthesis procedure employed in this study consisted of using zinc acetate as a precursor, and various plant species as a source of reducing, stabilizing and capping agents. The novelty in the present biosynthesis was the use of desert plants species of invasive or medicinal properties, notably *Thymelaea hirsuta* L., *Aloe vera* L., *Retama monosperma* L., and *Peganum harmala* L. The respective bio-ZnONPs consist of *Thymhirs*.bio-ZnONP, *Aloever*.bio-ZnONP, *Retam*.bio-ZnONP, and *harm*.bio-ZnONP. The measurement of the UV-vis absorption spectrum confirmed the nanosized property of the nascent bio-ZnONPs. The UV-vis absorption spectra of biosynthesized ZnONPs from each plant species showed close maximum absorption peaks in the range 340-400 nm, which is characteristic for ZnONPs. FTIR analysis allowed to ascertain the purity and nature of ZnONPs, and identify the phytochemicals and functional groups on the surface of ZnONPs. The phytochemicals such as alcohols, phenols, amines, and carboxylic acids interact with zinc acetate, and help in the stabilization of the bio-ZnONPs. Phytocompounds, including phenolic acids and flavonoids may potentially act as reducing, stabilizing and capping agents during the biosynthesis of ZnONPs. *P. harmala*, *T. hirsute*, *A. vera* and *R. monosperma* L. showed different phenolic compounds identified by HPLC-MS, mainly quinic acid, gallic acid,

transferulic acid, rutin, luteolin-7-o-glucoside, 3,4-di-O-caffeoyquinic acid, caffeic acid, naringenin, quercetin, protocatechuic acid, quercetin (quercetin-3-o-rhamonosic), rosmarinic acid, catechin and epicatechin, salviolinic acid, hyperoside(quercetin-3-o-galactoside), apegenin-7-o-glucoside, trans cinnamic, chlorogenic acid, syringic acid and cirsiolol. Furthermore, the variation in plants composition among different studied species plays a crucial role in determining the structural stability, reactivity, and potential applications of the synthesized nanoparticles. In addition, the various phytochemicals and compounds present in the plant extracts, such as flavonoids, tannins, alkaloids, terpenoids, amines, carboxylic acids, sugars, and ketones and phenolic compounds interact with the particle surface, and aid in the stabilization of ZnONPs, thus acting as natural capping, reducing, and stabilizing agents, preventing the agglomeration of ZnONPs by forming a protective layer around them. This organic coating enhances colloidal stability, reduces particle aggregation, and improves the dispersibility of the nanoparticles in different solvents [31, 32]. Previous reports involving other plants including *Cannabis sativa*, *Ceratonia siliqua* and *Artemisia vulgaris* also showed the role of flavonoids, steroids, coumarins, alkaloids, glycosides, anthraquinones, monoterpenes, diterpenes, phenolic acids, and phenols, present in plants' extracts, in stabilizing the biosynthesized ZnONPs [12, 14, 33]. The phenolic acids and flavonoids play crucial roles in ZnONPs synthesis as they can act simultaneously as reducing agents, stabilizing agents, and capping agents. For instance, the phenolic hydroxyl groups of flavonoids can donate electrons, while the phenolic groups containing in phenolic acids are capable of donating electrons, which facilitate the reduction of metal ions by transferring electrons to the metal ions, thereby promoting the formation of NPs. Later, these polyphenolic compounds attach to NPs' surface, where their hydroxyl groups and aromatic rings interact via hydrogen bonding and π - π stacking, preventing NP agglomeration and maintaining stability in solution. Then, these compounds can also form a protective layer around the NPs surface, which helps control their size and shape, and provides additional stability by preventing further growth or aggregation.

Furthermore, the presence of these phytochemicals influences the surface chemistry of the nanoparticles, affecting their charge and interaction with surrounding media. This stabilization not only extends the shelf life of the ZnONPs, but also enhances their biocompatibility and functionality for different applications including medicine and pharmacology. In addition to these biochemicals that confer biological properties to studied plants species [29, 30, 34], interesting paramagnetic properties were also revealed for the biologically synthesized ZnONPs.

In the preclinical study, the bio-ZnONPs interacted differently with the tested *in vitro* bacterial, yeast and fungal microorganisms. For evaluation, a strong antimicrobial activity was indicative by the inhibition zones with diameters of 15 mm or more. This suggests that the NPs are highly effective in inhibiting the growth of the tested microorganisms within a significant radius from the disc. A moderate antimicrobial activity consisted of the inhibition zones ranging from 10 mm to 14 mm, indicating that while there is an effect, it might not be as potent or widespread as with stronger antimicrobial agents; while weak antimicrobial activity was referred to the inhibition zones with diameters less than 10 mm, suggesting that the NPs have limited effectiveness in inhibiting microbial growth or that the concentration used may not be sufficient to produce a robust inhibitory effect.

Thymhirs.bio-ZnONP was the most efficient against the bacterial strain *Staphylococcus aureus* ATCC25923, and the yeast *Candida albicans* ATCC90028, as well as the fungal strains *Aspergillus flavus* and *Aspergillus fumigatus*. The *Aloever*.bio-ZnONP had the most inhibitory effect against the bacterial strain *Micrococcus luteus* NCIMB 8166, and the yeast *C. albicans*, *C. krusei* and *C. neoformans*. The *Aloever*.bio-ZnONP also showed an efficient antifungal activity against all strains of *Aspergillus*, especially *A. flavus* and *A. fumigatus*. The *Retam*.bio-ZnONP also displayed high inhibition against the bacterial strains *S. aureus*, *M. luteus* and *S. enterica serotype Typhimurium*, and the yeast *C. albicans*, associated antifungal bioactivity against *A. flavus*. The *harm*.bioZnONP exhibited antibacterial activity against *S. aureus* and *M. luteus*, *C. neoformans*, and all fungal species; *A. flavus*, *A. niger* and *A. fumigatus*, especially against *A. fumigatus*. Overall findings confirm the efficient antibacterial, antimicrobial and antifungal properties of the bio-ZnONPs.

The results of the current study agree with other studies that reported the antimicrobial activity of ZnONPs against various pathogens, such as *E.Coli*, *B. subtilis*, *Salmonella*, *Listeria monocytogenes*, and *Staphylococcus aureus* [15, 33, 35]. Some of the proposed mechanisms associated with the antibacterial activity of ZnONPs included the disruption of the pathogen cell membrane, and the induction of intracellular injuries, as a result of the induction of oxidative injury, and the hyper-generation of reactive oxygen species (ROS). In a previous study [35], the green synthesis of multifunctional ZnONPs using *P. caerulea*. showed an important inhibition zone of the growth of pathogenic microbes, thus suggesting the potential biomedical capability of ZnONPs. In another study, biologically synthesized AgNPs exhibited an inhibitory effect on microbes without any toxic effect on human, and mouse cells that may indicate an outstanding potential to discriminate between potential pathogens and mammalian cells [4].

The findings in this study suggest the plants species as a useful and efficient tool in the biosynthesis of antimicrobial bio-ZnONPs, which can be ultimately applied in several applications. Besides, the differential antimicrobial response of *Thymhirs.bio-ZnONP*, *Aloever.bio-ZnONP*, *Retam.bio-ZnONP*, and *harm.bio-ZnONP* towards the various microorganisms suggests their potential use as bio-nanoproducts in several domains of application. Combining the phytochemistry to appropriate processing techniques and nanosynthesis process may ensure the preparation of the end nanoproducts. The plants-based NPs may improve the potential function and efficacy of the plants' bioactive compounds in medicinal practices, or sustainable industrial applications. For example, *T. hirsuta* L. based ZnONP may ensure better clinical effectiveness. *A. vera* derived ZnONP may be useful in food or medication industry, while ZnONP may improve its medicinal value and commercial uses [36, 37]. *R. monosperma* derived ZnONPs may be useful in skin restoration and cicatrization [38]. Another use of *R. monosperma* can be a source of natural fibers in fibers industry. These vegetable fibers have many advantages, notably their availability, easy extractability, biodegradability, safety, ecofriendly, and recyclability. Therefore, when these properties are added to the antimicrobial properties of ZnONP, the resulting nanoproduct may offer additional advantages in fibers production [39]. The most recent pharmaceutical uses of *P. harmala* included antimicrobial effects, antineoplasm and beneficial effects on several organ systems such as cardiovascular, nervous, endocrine, gastrointestinal and respiratory systems. Besides, their content of phenolic compounds is valued for antioxidant capacity, thus suggesting their high potential in pharmacological activity. However, combined effects between high potential medicinal herb and physico-chemical and biological properties of NPs may increase efficacy and safety.

Nonetheless, more research is needed to develop efficient processing techniques that can preserve or enhance the bioactive properties, which are naturally present in plants. This may improve the product quality and safety. Also, the industries involved in processing plants species need to check both safety and toxicological outcomes of bio-engineered nanomaterials in food and medicine applications.

Lipophilicity, druglikeness and pharmacokinetic properties of the phenolic acids and flavonoids of *Thymelaea hirsuta* L., *Aloe vera* L., *Retama monosperma* L. and *Peganum harmala* L. are shown in Table 5. The assessment of such parameters towards drug design and development is crucial to avoid any drug failures at the advanced stages [26, 27, 29, 30, 34]. The majority of these phytochemicals meet the Lipinski rule and have acceptable druggability. Based on the flexibility (flex), insaturation (insatu), insolubility (insolu),

lipophilicity (lipo), molecular size (size), and polarity (pola), the studied compounds possessed acceptable oral bioavailability scores varying from 0.11 to 0.85. This supported their potential bioactivities. Both blood-brain-barrier (BBB) permeation and gastro-intestinal (GI) absorption have been explored and used for designing of the egg-model (Figure 5). Most of identified phytochemicals have acceptable skin permeation and are not predicted to be substrates of P-glycoprotein (P-gp), In fact, Log Kp values varied between -5.66 and -9.15 . As cytochromes P450 (such as CYP1A2, CYP2C9, CYP2C19, CYP2D6 and CYP3A4) play key role in metabolism and excretion of drugs [29, 30, 40]. Their eventual inhibition was also predicted. Table 4 exhibited that while each of these studied CYPs was inhibited by only few compounds, CYP2C19 was not inhibited by any of the phytochemicals. These findings indicate that these phytochemicals are safe regarding metabolism and excretion. The synthetic accessibility was found to range between 1.07 and 5.28, which indicate that these compounds are easy to synthesize [29, 30, 40].

It was predicted that all these phytochemicals had negative but varied binding affinities to each of 1JII, 2QZW and 2UVO receptors (Table 5). These affinities reached -10.5 , -10.0 and -8.4 kcal/mol for 1JII, 2QZW and 2UVO, respectively. Variations in binding affinities was reported to be the result of both ligand and receptors 3D chemical structures [26, 29, 34]. These best binding scores were predicted for the phytochemicals no. 12, 8 and 16 respectively (Tables 5 and 6). These phytochemicals possessed several biological effects, which includes strong antimicrobial activity [30, 41], promotion of cell apoptosis, inhibition of several cancer cells such as HeLa and MCF7 [30, 42]. Many identified phytochemicals were predicted to settle acceptable molecular interactions with each of the studied receptors and included up to 9 conventional H-bonds. For instance, compound no. 8 established 9 conventional H-bonds, which have been supported with van der Waals and Pi-alkyl bonds (Figure 6) as they increase the complex stability of the complex [26, 27, 29]. These interactions concerned LYS49, SER89, ASN160, LYS178, SER336, GLY87, PRO4, ILE338, and THR166. The latter was complexed with the compound no. 8 via 3 conventional H-bonds and was the closest interacting residue (2.150 \AA). Deep embedding ($<2.5 \text{ \AA}$) of the ligands was reported to be associated with several biological effects such as including anticancer anti-inflammatory, and antimicrobial potentials [40, 43].

Deep embedding of distances less than 2.5 \AA similarly to findings of the current study have been largely reported to be involved in different bioactivities including antioxidant, antiproliferative, anti-inflammatory, and antimicrobial effects [24, 40, 44]. It could be deduced from the binding affinities, the established molecular interactions of the identified

compounds and their deep embedding that the potential antimicrobial effect is thermodynamically possible. This was already been highlighted through *in vitro* findings. Thus, supporting the promising health promotion and beneficial effects of products and phototherapeutic potential of medicinal plants [24, 40, 43]. Nonetheless, several limitations hinder their large-scale application and reproducibility. Plant-derived ZnONPs involve variable synthesis processes that also depends on the biochemical composition of the plant extract, which can vary due to factors like plant species, growth conditions, and extraction methods. This variability can lead to inconsistent nanoparticle properties, such as size, shape, and stability. Another limitation of plant-mediated ZnONPs consists in the limited control over particle size and morphology- compared to chemical or physical synthesis methods, thus resulting in a broader particle size distribution and irregular morphologies [45]. Plant-derived ZnONPs may have lower stability than chemically synthesized ones due to weaker capping by organic compounds, which may reduce their effectiveness over time. [46]. Besides, plant extracts contain various organic compounds, which may introduce impurities into the ZnONPs, which can affect their biological activities and applications, requiring additional purification steps. Industrial-scale synthesis requires consistent precursor concentrations, reaction times, and temperatures, which are difficult to achieve with plant extracts. Also, there is limited mechanistic understanding about the exact mechanisms by which plant metabolites reduce and stabilize ZnONPs. This gap in knowledge challenges the optimization of the synthesis process of nanoparticles for specific applications. In this context, additional research is required to investigate the nanoparticle stability in varied media, including pH variations, presence of enzymes or proteins in biological fluids, and other relevant factors that might affect their efficacy as antimicrobial agents. We suggest developing several methods and strategies for the optimization of reaction parameters, such as fine-tuning reaction conditions such as temperature, pH, reaction time, and precursor concentrations to ensure consistent nanoparticle size, shape, and surface properties. We also recommend implementing continuous flow reactors can improve scalability by maintaining precise control over reaction conditions and enhancing reproducibility. An additional strategy is employing the microfluidic platforms to enable precise mixing of reactants at a microscale, promoting uniform nanoparticle synthesis and minimizing batch-to-batch variation. nanoparticle characterization: implementing robust characterization techniques at various stages of synthesis to monitor nanoparticle properties and ensure batch-to-batch consistency. Also, we suggest integrating automated systems for nanoparticle synthesis and purification in order to reduce labor-intensive tasks, minimize human error, and ensure consistent product

quality during scale-up. By incorporating these methods and strategies, we can effectively scale up the synthesis of plant-based nanoparticles while preserving their integrity and antimicrobial properties, facilitating their translation into practical biomedical and pharmaceutical applications. Regarding scale-up feasibility, exploring the potential for scaling up production is essential for practical application, while maintaining their integrity and antimicrobial properties.

Addressing safety protocols and environmental impacts associated with scaled-up production should be considered, including waste management and disposal of reactants and by-products. We also suggest engaging in collaborations with industry partners, research institutions, and regulatory bodies to validate scalability, safety, and efficacy of scaled-up nanoparticle synthesis processes. Further research is needed to investigate the potential toxicity and biocompatibility of plant-derived ZnONPs that are often considered biocompatible. Touching upon the biocompatibility and safety profiles of these nanoparticles in relation to their intended biomedical applications would add depth. This includes considerations of cytotoxicity, immunogenicity, and long-term effects that might influence their use in clinical settings. On the other hand, we need to investigate potential toxicity, and ensure the safe use of NPs in biomedical and environmental applications. For example, ZnONPs synthesized from *Eclipta prostrata* exhibited cytotoxic effects on human lung fibroblast cells at higher concentrations [47].

CONCLUSION

Overall, this study elucidated a fast, cost-effective, and environmentally friendly process for ZnONPs biosynthesis, using plant species that grow in temperate desert and Mediterranean surrounding areas; *Thymelaea hirsuta* L., *Aloe vera* L., *Retama monosperma* L. and *Peganum harmala* L., but are not generally valuable nor valorized. The biologically synthesized nanoparticles can be considered as valued nanoproducts to develop more efficient antimicrobial agents against drug resistant microbes, or alternatively to develop functional foods and pharmaceutical drugs. The pharmacokinetic characteristics of the identified compounds may explain the *in vitro* antimicrobial activities that may result from the potential molecular interactions of ZnONPs biosynthesis associated phytochemicals with some commonly antimicrobial targeted receptors.

ACKNOWLEDGMENTS

The authors want to acknowledge the Deanship of Scientific Research – University of Ha'il for supporting this study (project no. RG-23 124).

Conflicts of interest: Authors declare no conflicts of interest.

Funding: This research has been funded by Deanship of Scientific Research – University of Ha'il through project number RG-23 124.

Data availability: The data supporting the findings of this study are available upon request.

Submitted: 25 January 2025

Accepted: 9 May 2025

Published online: 15 May 2025

REFERENCES

1. Singh P, Kim YJ, Zhang D, Yang DC (2016) Biological Synthesis of Nanoparticles from Plants and Microorganisms. Trends Biotechnol 34:588–599.
<https://doi.org/10.1016/J.TIBTECH.2016.02.006>
2. Tiwari V, Mishra N, Gadani K, et al (2018) Mechanism of anti-bacterial activity of zinc oxide nanoparticle against Carbapenem-Resistant *Acinetobacter baumannii*. Front Microbiol 9:. <https://doi.org/10.3389/FMICB.2018.01218/FULL>
3. Sundrarajan M, Ambika S, Bharathi K (2015) Plant-extract mediated synthesis of ZnO nanoparticles using *Pongamia pinnata* and their activity against pathogenic bacteria. Advanced Powder Technology 26:1294–1299.
<https://doi.org/10.1016/J.APT.2015.07.001>
4. Raveendran P, Fu J, Wallen SL (2003) Completely “Green” Synthesis and Stabilization of Metal Nanoparticles. J Am Chem Soc 125:13940–13941.
https://doi.org/10.1021/JA029267J/SUPPL_FILE/JA029267JSI20030324_031335.P

DF

-
5. Ahmad S, Zainab, Ahmad H, et al (2022) Green synthesis of gold nanoparticles using *Delphinium Chitralense* tuber extracts, their characterization and enzyme inhibitory potential. *Brazilian Journal of Biology* 82:. <https://doi.org/10.1590/1519-6984.257622>
 6. Azizi S, Mohamad R, Bahadoran A, et al (2016) Effect of annealing temperature on antimicrobial and structural properties of bio-synthesized zinc oxide nanoparticles using flower extract of *Anchusa italica*. *J Photochem Photobiol B* 161:441–449. <https://doi.org/10.1016/J.JPHOTOBIOB.2016.06.007>
 7. Rocha MB da C, Araújo TR de, Medeiros RLB de A, et al (2021) Recent advances (2016 - 2020) in green synthesis of metal oxide nanoparticles: An overview. *Research, Society and Development* 10:e399101623406. <https://doi.org/10.33448/RSD-V10I16.23406>
 8. Khalil AT, Ovais M, Ullah I, et al (2017) *Sageretia thea* (Osbeck.) mediated synthesis of zinc oxide nanoparticles and its biological applications. *Nanomedicine (Lond)* 12:1767–1789. <https://doi.org/10.2217/NNM-2017-0124>
 9. Anand Raj LFA, Jayalakshmy E (2015) Biosynthesis and characterization of zinc oxide nanoparticles using root extract of *Zingiber officinale*. *Oriental Journal of Chemistry* 31:51–56. <https://doi.org/10.13005/OJC/310105>
 10. Gupta M, Tomar RS, Kaushik S, et al (2018) Effective antimicrobial activity of green ZnO nano particles of *Catharanthus roseus*. *Front Microbiol* 9:392294. <https://doi.org/10.3389/FMICB.2018.02030/BIBTEX>
 11. Fakhari S, Jamzad M, and HKF-G chemistry letters, (2019) Green synthesis of zinc oxide nanoparticles: a comparison. Taylor & FrancisS Fakhari, M Jamzad, H Kabiri

-
- FardGreen chemistry letters and reviews, 2019•Taylor & Francis 12:19–24.
<https://doi.org/10.1080/17518253.2018.1547925>
12. Karmous I, Vaidya S, Dimkpa C, et al (2023) Biologically synthesized zinc and copper oxide nanoparticles using *Cannabis sativa* L. enhance soybean (*Glycine max*) defense against *fusarium virguliforme*. Pestic Biochem Physiol 194:105486.
<https://doi.org/10.1016/J.PESTBP.2023.105486>
 13. Karmous I, Taheur F Ben, Zuverza-Mena N, et al (2022) Phytosynthesis of Zinc Oxide Nanoparticles Using *Ceratonia siliqua* L. and Evidence of Antimicrobial Activity. Plants 11:3079. <https://doi.org/10.3390/PLANTS11223079/S1>
 14. Karmous I, Elmer WH, Zuverza-Mena N, et al (2025) Plant-engineered ZnO and CuO nanoparticles exhibit pesticidal activity and mitigate *Fusarium* infestation in soybean: A mechanistic understanding. Plant Physiology and Biochemistry 221:109672. <https://doi.org/10.1016/J.PLAPHY.2025.109672>
 15. Ghasemi F, Jalal R (2016) Antimicrobial action of zinc oxide nanoparticles in combination with ciprofloxacin and ceftazidime against multidrug-resistant *Acinetobacter baumannii*. J Glob Antimicrob Resist 6:118–122.
<https://doi.org/10.1016/J.JGAR.2016.04.007>
 16. Venkatasubbu GD, Baskar R, Anusuya T, et al (2016) Toxicity mechanism of titanium dioxide and zinc oxide nanoparticles against food pathogens. Colloids Surf B Biointerfaces 148:600–606. <https://doi.org/10.1016/J.COLSURFB.2016.09.042>
 17. Fowsiya J, Madhumitha G, Al-Dhabi NA, Arasu MV (2016) Photocatalytic degradation of Congo red using *Carissa edulis* extract capped zinc oxide nanoparticles. J Photochem Photobiol B 162:395–401.
<https://doi.org/10.1016/J.JPHOTOBIO.2016.07.011>

-
18. Dobrucka R, Długaszewska J (2016) Biosynthesis and antibacterial activity of ZnO nanoparticles using *Trifolium pratense* flower extract. Saudi J Biol Sci 23:517–523. <https://doi.org/10.1016/J.SJBS.2015.05.016>
 19. Badawy A, Hassanean H, Ibrahim AK, et al (2021) Isolates From *Thymelaea Hirsuta* Inhibit Progression Of Hepatocellular Carcinoma *In Vitro* And *In Vivo*. Nat Prod Res 35:1799–1807. <https://doi.org/10.1080/14786419.2019.1643859>
 20. Eshun K, He Q (2004) Aloe vera: a valuable ingredient for the food, pharmaceutical and cosmetic industries--a review. Crit Rev Food Sci Nutr 44:91–96. <https://doi.org/10.1080/10408690490424694>
 21. Kuete V (2014) Physical, Hematological, and Histopathological Signs of Toxicity Induced by African Medicinal Plants. Toxicological Survey of African Medicinal Plants 635–657. <https://doi.org/10.1016/B978-0-12-800018-2.00022-4>
 22. Shahrajabian M, Sun W, Phytoscience QC-C, 2021 undefined (2021) Improving health benefits with considering traditional and modern health benefits of *Peganum harmala*. SpringerMH Shahrajabian, W Sun, Q ChengClinical Phytoscience, 2021•Springer 7:. <https://doi.org/10.1186/s40816-021-00255-7>
 23. Iranshahy M, Bazzaz SF, Haririzadeh G, et al (2019) Chemical composition and antibacterial properties of *Peganum harmala* L. Avicenna J Phytomed 9:530. <https://doi.org/10.22038/AJP.2019.13382>
 24. Akacha A, Badraoui R, Rebai T, Zourgui L (2022) Effect of *Opuntia ficus indica* extract on methotrexate-induced testicular injury: a biochemical, docking and histological study. J Biomol Struct Dyn 40:4341–4351. <https://doi.org/10.1080/07391102.2020.1856187>

-
25. Badraoui R, Adnan M, Bardakci F, Alreshidi MM (2021) Chloroquine and Hydroxychloroquine Interact Differently with ACE2 Domains Reported to Bind with the Coronavirus Spike Protein: Mediation by ACE2 Polymorphism. *Molecules* 2021, Vol 26, Page 673 26:673. <https://doi.org/10.3390/MOLECULES26030673>
 26. Ben Saad H, Frikha D, Bouallegue A, et al (2023) Mitigation of Hepatic Impairment with Polysaccharides from Red Alga *Albidum corallinum* Supplementation through Promoting the Lipid Profile and Liver Homeostasis in Tebuconazole-Exposed Rats. *Pharmaceuticals (Basel)* 16:. <https://doi.org/10.3390/PH16091305>
 27. Mhadhbi N, Dgachi S, Belgacem S, et al (2023) Design, theoretical study, druggability, pharmacokinetics and properties evolution of a new organo-bromocadmte compound as prospective anticancer agent. *JMoSt* 1274:134439. <https://doi.org/10.1016/J.MOLSTRUC.2022.134439>
 28. Elkahoui S, Jamal A, Abbes W Ben, et al (2024) Investigation of the Valorization of Methanolic Extract of *Punica granatum* L. Peel in Terms of Phytochemical, Trace Element, Antioxidant Activities and ADMET Profile of Active Compounds. *Pol J Environ Stud* 33:2587–2602. <https://doi.org/10.15244/PJOES/175022>
 29. Badraoui R, Siddiqui AJ, Bardakci F, Ben-Nasr H (2023) Ethnopharmacology and Ethnopharmacognosy Current Perspectives and Future Prospects. *Ethnobotany and Ethnopharmacology of Medicinal and Aromatic Plants: Steps Towards Drug Discovery* 115–128. <https://doi.org/10.1201/B22842->
 30. Bédoui I, Nasr H Ben, Ksouda K, et al (2024) Phytochemical Composition, Bioavailability and Pharmacokinetics of *Scorzonera undulata* Methanolic Extracts: Antioxidant, Anticancer, and Apoptotic Effects on. journals.sagepub.com I Bédoui, HB Nasr, K Ksouda, W Ayadi, N Louati, M Chamkha, S Choura, J

GargouriPharmacognosy Magazine, 2024•journals.sagepub.com 20:218–229.

<https://doi.org/10.1177/09731296231207231>

31. Ovais M, Khalil AT, Islam NU, et al (2018) Role of plant phytochemicals and microbial enzymes in biosynthesis of metallic nanoparticles. *Appl Microbiol Biotechnol* 102:6799–6814. <https://doi.org/10.1007/S00253-018-9146-7>
32. Pradeep M, Kruszka D, Kachlicki P, et al (2022) Uncovering the Phytochemical Basis and the Mechanism of Plant Extract-Mediated Eco-Friendly Synthesis of Silver Nanoparticles Using Ultra-Performance Liquid Chromatography Coupled with a Photodiode Array and High-Resolution Mass Spectrometry. *ACS Sustain Chem Eng* 10:562–571. https://doi.org/10.1021/acssuschemeng.1c06960/asset/images/large/sc1c06960_0008.jpeg
33. Karmous I, Taheur F Ben, Zuverza-Mena N, et al (2022) Phytosynthesis of Zinc Oxide Nanoparticles Using *Ceratonia siliqua* L. and Evidence of Antimicrobial Activity. *Plants* 11:3079. <https://doi.org/10.3390/PLANTS11223079/S1>
34. Rahmouni F, Hamdaoui L, Saoudi M, et al (2024) Antioxidant and antiproliferative effects of *Teucrium polium* extract: computational and in vivo study in rats. *Toxicol Mech Methods* 34:495–506. <https://doi.org/10.1080/15376516.2023.2301670>
35. Rajeshkumar S, Santhoshkumar J, Shamugam VK (2017) Synthesis of zinc oxide nanoparticles using plant leaf extract against urinary tract infection pathogen. *Resource-Efficient Technologies* 459–465. <https://doi.org/10.18799/24056529/2017/4/172>

-
36. Ahlawat KS, Khatkar BS (2011) Processing, food applications and safety of aloe vera products: a review. *J Food Sci Technol* 48:525–533.
<https://doi.org/10.1007/S13197-011-0229-Z>
37. Baruah A, Bordoloi M, Deka Baruah HP (2016) Aloe vera: A multipurpose industrial crop. *Ind Crops Prod* 94:951–963.
<https://doi.org/10.1016/J.INDCROP.2016.08.034>
38. Zefzoufi M, Fdil R, Bouamama H, et al (2021) Effect of extracts and isolated compounds derived from *Retama monosperma* (L.) Boiss. on anti-aging gene expression in human keratinocytes and antioxidant activity. *J Ethnopharmacol* 280.
<https://doi.org/10.1016/J.JEP.2021.114451>
39. Aizi D, Biotechnology MH-AJ of, 2015 undefined (2015) Extraction and characterization of *Retama monosperma* fibers. *MK Harche African Journal of Biotechnology*, 2015•ajol.info 14:2644–2651.
<https://doi.org/10.5897/AJB2015.14812>
40. Alreshidi M, Abdulhakeem MA, Badraoui R, et al (2023) *Pulicaria incisa* (Lam.) DC. as a Potential Source of Antioxidant, Antibacterial, and Anti-Enzymatic Bioactive Molecules: Phytochemical Constituents, In Vitro and In Silico Pharmacological Analysis. *Molecules* 2023, Vol 28, Page 7439 28:7439.
<https://doi.org/10.3390/MOLECULES28217439>
41. Bajko E, Kalinowska M, Borowski P, et al (2016) 5-O-Caffeoylquinic acid: A spectroscopic study and biological screening for antimicrobial activity. *LWT* 65:471–479. <https://doi.org/10.1016/J.LWT.2015.08.024>
42. Liu MM, Ma RH, Ni ZJ, et al (2020) Apigenin 7-O-glucoside promotes cell apoptosis through the PTEN/PI3K/AKT pathway and inhibits cell migration in

-
- cervical cancer HeLa cells. *Food Chem Toxicol* 146:.
<https://doi.org/10.1016/J.FCT.2020.111843>
43. Kraiem M, Ben Hamouda S, Eleroui M, et al (2024) Anti-Inflammatory and Immunomodulatory Properties of a Crude Polysaccharide Derived from Green Seaweed *Halimeda tuna*: Computational and Experimental Evidences. *Marine Drugs* 2024, Vol 22, Page 85 22:85. <https://doi.org/10.3390/MD22020085>
44. Othman IMM, Gad-Elkareem MAM, Radwan HA, et al (2021) Synthesis, Structure-Activity Relationship and in silico Studies of Novel Pyrazolothiazole and Thiazolopyridine Derivatives as Prospective Antimicrobial and Anticancer Agents. *ChemistrySelect* 6:7860–7872. <https://doi.org/10.1002/SLCT.202101622>
45. Rajiv P, Rajeshwari S, Venckatesh R (2013) Bio-fabrication of zinc oxide nanoparticles using leaf extract of *Parthenium hysterophorus* L. and its size-dependent antifungal activity against plant fungal pathogens. *Spectrochim Acta A Mol Biomol Spectrosc* 112:384–387. <https://doi.org/10.1016/J.SAA.2013.04.072>
46. Bhuyan T, Mishra K, Khanuja M, et al (2015) Biosynthesis of zinc oxide nanoparticles from *Azadirachta indica* for antibacterial and photocatalytic applications. *Mater Sci Semicond Process* 32:55–61.
<https://doi.org/10.1016/J.MSSP.2014.12.053>
47. Kalpana VN, Devi Rajeswari V (2018) A Review on Green Synthesis, Biomedical Applications, and Toxicity Studies of ZnO NPs. *Bioinorg Chem Appl* 2018:3569758. <https://doi.org/10.1155/2018/3569758>

TABLES AND FIGURES WITH LEGENDS

Table 1. Granulometry measurement of particle diameter of ZnONP

Bio-ZnONP	d (0.1) μm	nm	d (0.5) μm	nm	d (0.9) μm	nm
Thymhirs.bio-ZnONP	0.392	392	0.543	543	1.212	1212
Aloever.bio-ZnONP	0.410	410	0.742	742	1.688	1688
Retam.bio-ZnONP	0.742	742	0.980	980	1.666	1666
Harm.bio-ZnONP	0.255	255	0.348	348	0.589	589

Table 2. Qualitative and quantitative (ppm) of phenolic acids and flavonoids by HPLC-MS of extracts of *Thymelaea hirsuta* L., *Aloe vera* L., *Retama monosperma* L. and *Peganum harmala* L.

Phenolic compounds	<i>Thymelaea hirsuta</i> L.	<i>Aloe vera</i> L.	<i>Retama monosperma</i> L.	<i>Peganum harmala</i> L.
1 Quinic acid	137.725	141.767	151.37	182.515
2 Gallic acid	0.153	0.106	0.051	0.162
3 Protocatechuic acid	0	2.84	0	0
4 p-coumaric acid	0.13	0	0.025	0.294
5 Trans-ferulic acid	0.014	0.08	0	0.23
6 Rutin	0.225	0.53	0.194	0.452
7 Luteolin-7-O-glucoside	0	2.205	0	4.414
8 3,4-di-O-caffeoyquinic acid	0	0	0.151	0.591
9 Caffeic acid	0	1.007	0	0.114
10 Salviolinic acid	0	1.167	0	0
11 Quercetin	0.022	0	0	0
12 Quercetin (quercetin-3-o-rhamonosic)	0	6.377	0	0
13 Hyperoside(quercetin-3-o-galactoside)	0	0.556	0.157	0
14 Naringin	0	2.623	0	0
15 Naringenin	0	1.321	0	6.978

16	Apegenin-7-o-glucoside	0.262	4.282	0.017	2.616
17	Apegenin	0	0.47	0	5.409
18	Rosmarinic acid	0	0.099	0	0
19	Acacetin	0	0	0	0
20	trans cinnamic acid	0	0.309	0	0.06
21	Cirsiliol	0.712	11.452	0.287	0.734
22	(+)-Catechin	0	9.723	0	0
23	Epicatechin	0	0.878	0	0
24	Chlorogenic acid	0	171.64	2.866	0
25	Syringic acid	0	0.366	0	0.076

EARLY ACCESS

Table 3. Antimicrobial activities (Inhibition diameter, mm) of *Thymhirs.bio-ZnONP*”, “*Aloever.bio-ZnONP*”, “*Retam. bio-ZnONP*” and “*harm. Bio-ZnONP*”.

Bacterial Strains	<i>Thymhirs.bio-</i>	<i>Aloever.bio-</i>	<i>Retam.bio-</i>	<i>harm.bio-</i>	<i>Plant extracts</i>			
	ZnONP	ZnONP	ZnONP	ZnONP	<i>T. hir.</i>	<i>A. ver.</i>	<i>R. mon.</i>	<i>P. har.</i>
<i>Staphylococcus aureus</i>	15±1.41 ^a	13±0.71 ^{ab}	11±0.71 ^b	13±0.71 ^{ab}	0±0 ^a	0±0 ^b	0.33±0.57 ^a	23±1.00 ^a
<i>Micrococcus luteus</i>	13±0.71 ^b	24±0.00 ^a	13±0.71 ^b	12±0.71 ^c	0±0 ^a	0±0 ^b	1±1.00 ^a	10±1.00 ^a
<i>Salmonella ent. ser. Typh.</i>	0 ^b	0 ^b	11±0.00 ^a	0 ^b	0±0 ^a	0±0 ^b	1.33±0.58 ^a	11.33±1.53 ^a
<i>Escherichia coli</i>	0	0	0	0	0±0 ^a	15±1.00 ^a	11±1.00 ^a	11±1.00 ^a
Yeast strains	Activity against yeast growth (Inhibition diameter, mm)							
<i>Candida albicans</i>	14±0.71 ^a	14±0.71 ^a	13±0.00 ^b	0 ^c	11±1.00 ^a	7.67±2.51 ^a	8.00±1.00 ^a	0.67±1.00 ^a
<i>Candida krusei</i>	0 ^b	12±0.71 ^a	0 ^b	0 ^b	0.0±0.0 ^b	8.0±1.73 ^a	0.00±0.00 ^b	0.00±0.00 ^a
<i>Candida neoformans</i>	0 ^c	11±0.00 ^b	0 ^c	16±0.71 ^a	0.0±0.0 ^b	8.0±1.00 ^a	0.00±0.00 ^b	11.33±0.58 ^a
Fungal strains	Antifungal activity (Inhibition diameter, mm)							
<i>Aspergillus flavus</i>	16±0.71 ^b	16±1.41 ^b	17±0.71 ^a	14±0.71 ^c	10.00±1.00 ^a	11.67±1.15 ^{ab}	8.00±1.00 ^a	11.00±1.00 ^a
<i>Aspergillus niger</i>	0 ^c	16±1.41 ^a	0 ^c	15±0.00 ^b	0.67±0.57 ^b	12.00±2.00 ^a	8.00±1.00 ^a	10.00±1.00 ^b
<i>Aspergillus fumigatus</i>	12±0.00 ^b	12±0.71 ^b	0 ^c	16±0.71 ^a	9.00±1.00 ^a	7.00±1.73 ^b	8.00±1.00 ^a	11.00±1.73 ^a

Bacterial strains consisted of *Staphylococcus aureus* (ATCC 25 923), *Micrococcus luteus* (NCIMB 8166), *Salmonella enterica serotype Typhimurium* (ATCC 1408) and *Escherichia coli* (ATCC35218). Yeast strains consisted of *Candida albicans* (ATCC90028), *Candida krusei* (ATCC6258) and *Candida neoformans* (ATCC14116). Fungal strains consisted of *Aspergillus flavus* (15UA005), *Aspergillus niger* (15UA006) and

Aspergillus fumigatus (ATCC204305), *T. hir.*, *A. ver.*, *R. mon.*, and *P. har.* referred to the assays using plant extracts, respectively, of *Thymelaea hirsuta* L., *Aloe vera* L., *Retama monosperma* L., and *Peganum harmala* L. The significance of the difference between microbial strains was determined using ANOVA ($\alpha=0.05$). Letters denote statistical difference between the types of ZnONPs, using the Duncan test ($\alpha=0.05$).

Table 4. Control assays of the antimicrobial activities (Inhibition diameter, mm) of Zinc acetate salt, and commercial antibiotics; Gentamicin (10 µg/mL) and Cycloheximide (10 µg/mL).

	Inhibitory diameter (mm)		
	Zinc acetate salt	Gentamicin	Cycloheximide.
Bacterial strains			
<i>Staphylococcus aureus</i>	11.33±1.52 ^a	25±2.00 ^a	*
<i>Micrococcus luteus</i>	11±0.577 ^a	22±2.00 ^b	*
<i>Salmonella en. ser. Typh.</i>	4±0.00 ^c	15.66±1.52 ^{ab}	*
<i>Escherichia coli</i>	10.67±2.08 ^b	22±2.00 ^b	*
Yeast strains			
<i>Candida albicans</i>	1.66±0.57 ^{ab}	*	21±1.0 ^a
<i>Candida krusei</i>	2.33±0.57 ^a	*	19.66±1.52 ^b
<i>Candida neoformans</i>	0.66±0.57 ^c	*	16.66±2.89 ^c
Fungal strains			
<i>Aspergillus flavus</i>	7±1.0 ^a	*	21.33±2.08 ^{ab}
<i>Aspergillus niger</i>	2±1.0 ^b	*	22.66±1.15 ^a
<i>Aspergillus fumigatus</i>	3±1.0 ^b	*	19±2.00 ^b

Bacterial strains consisted of *Staphylococcus aureus* (ATCC 25 923), *Micrococcus luteus* (NCIMB 8166), *Salmonella enterica serotype Typhimurium* (ATCC 1408) and *Escherichia coli* (ATCC35218). Yeast strains consisted of *Candida albicans* (ATCC90028), *Candida krusei* (ATCC6258) and *Candida neoformans* (ATCC14116). Fungal strains consisted of *Aspergillus flavus* (15UA005), *Aspergillus niger* (15UA006) and *Aspergillus fumigatus* (ATCC204305). The significance of the difference between microbial strains was determined using ANOVA ($\alpha=0.05$). Letters denote statistical difference between the types of ZnONPs, using the Duncan test ($\alpha=0.05$)

Table 5. Lipophilicity, druglikeness and pharmacokinetics of the phenolic acids and flavonoids (1-25) as identified by HPLC-MS extracts of *Thymelaea hirsuta* L., *Aloe vera* L., *Retama monosperma* L. and *Peganum harmala* L. based on their ADMET (for absorption, distribution, metabolism, excretion and toxicity) properties.

Entry	1	2	3	4	5	7	8	9	10	11	12	13	15	17	18	19	20	21	22	23	24	25	
	Lipophilicity & physicochemical properties																						
TPSA	118.22	97.99	77.76	57.53	66.76	190.28	211.28	77.76	184.98	131.36	190.28	210.51	86.99	90.9	144.52	79.9	37.3	109.36	110.38	110.38	164.75	75.99	
Log Po/w (iLOGP)	0.37	0.21	0.66	0.95	1.62	1.76	1.32	0.97	2.19	1.63	1.6	1.45	1.75	1.89	1.48	2.56	1.55	2.46	1.33	1.47	0.87	1.54	
Consensus Log Po/w	-1.66	0.21	0.65	1.26	1.36	0.15	0.8	0.93	2.66	1.23	0.22	-0.38	1.84	2.11	1.58	2.52	1.79	2.13	0.83	0.85	-0.39	0.99	
Log S (ESOL)	0.53	-1.64	-1.86	-2.02	-2.11	-3.65	-3.65	-1.89	-5.15	-3.16	-3.33	-3.04	-3.49	-3.94	-3.44	-4.14	-2.37	-4.12	-2.22	-2.22	-1.62	-1.84	
	Druglikeness & Medicinal chemistry																						
Lipinski	Yes	Yes	Yes	Yes	Yes	No	No	Yes	Yes	Yes	No	No	Yes	Yes	Yes	Yes	Yes	Yes	Yes	Yes	Yes	Yes	
Bioavailability score	0.56	0.56	0.56	0.85	0.85	0.17	0.11	0.56	0.11	0.55	0.17	0.17	0.55	0.55	0.56	0.55	0.85	0.55	0.55	0.55	0.55	0.11	0.56
Leadlikeness	1	1	1	1	1	1	2	1	3	0	1	1	0	0	1	0	1	0	0	0	1	1	
Synthetic accessibility	3.34	1.22	1.07	1.61	1.93	5.17	4.86	1.81	4.18	3.23	5.28	5.32	3.01	2.96	3.38	2.98	1.67	3.32	3.5	3.5	4.16	1.7	
	Pharmacokinetics																						
GI absorption	Low	High	High	High	High	Low	Low	High	Low	High	Low	Low	High	High	Low	High	High	High	High	High	High	Low	High
BBB permeant	No	No	No	Yes	Yes	No	No	No	No	No	No	No	No	No	No	No	Yes	No	No	No	No	No	No
P-gp substrate	No	No	No	No	No	Yes	Yes	No	No	No	No	No	Yes	No	No	No	No	No	Yes	Yes	No	No	
CYP1A2	No	No	No	No	No	No	No	No	No	Yes	No	No	Yes	Yes	No	Yes	No	Yes	No	No	No	No	
CYP2C19	No	No	No	No	No	No	No	No	No	No	No	No	No	No	No	No	No	No	No	No	No	No	No
CYP2C9	No	No	No	No	No	No	No	No	Yes	No	No	No	No	No	No	Yes	No	Yes	No	No	No	No	
CYP2D6	No	No	No	No	No	No	No	No	No	Yes	No	No	No	Yes	No	Yes	No	Yes	No	No	No	No	
CYP3A4	No	Yes	Yes	No	No	No	No	No	No	Yes	No	No	Yes	Yes	No	Yes	No	Yes	No	No	No	No	
Log Kp (skin)	-9.15	-6.84	-6.42	-6.26	-6.41	-8	-8.37	-6.58	-6.53	-7.05	-8.42	-8.88	-6.17	-5.8	-6.82	-5.66	-5.69	-6.14	-7.82	-7.82	-8.76	-6.77	
TPSA: Topological polar surface area; GI: Gastro-intestinal; BBB: Blood-brain-barrier; P-gp: P-glycoprotein; CYP: Cytochrome P450																							

Table 6. Binding energy of the phenolic acids and flavonoids (1-25) as identified by HPLC-MS extracts of *Thymelaea hirsuta* L., *Aloe vera* L., *Retama monosperma* L. and *Peganum harmala*. L. and the 3 targeted receptors: 1JIJ, 2QZW and 2UVO for TyrRS from *Staphylococcus aureus*, aspartic proteinase from *Candida albicans*, and wheat germ agglutinin (2UVO), respectively.

Receptor / Ligand	Binding energy (kcal/mol)		
	1JIJ	2QZW	2UVO
1	-7.1	-6.1	-6.0
2	-7.3	-5.8	-5.5
3	-7.0	-5.7	-5.8
4	-6.5	-6.0	-5.2
5	-6.9	-6.4	-5.1
6	-9.5	-8.8	-7.6
7	-9.5	-9.9	-7.8
8	-9.4	-10.0	-6.9
9	-7.3	-6.4	-6.0
10	-9.7	-9.9	-7.4
11	-9.9	-8.2	-7.2
12	-10.5	-8.4	-7.4
13	-9.4	-8.8	-7.4
14	-8.6	-8.8	-8.4
15	-9.4	-8.2	-7.1
16	-9.1	-9.1	-8.4
17	-9.5	-8.2	-7.1
18	-7.6	-8.4	-6.5
19	-9.5	-8.3	-7.0
20	-6.3	-6.0	-5.4
21	-8.7	-8.5	-7.1
22	-9.2	-8.1	-7.1
23	-9.1	-8.4	-7.4
24	-9.0	-8.8	-6.8
25	-7.0	-5.9	-5.2

Table 7. Interactions, bond category and closest interacting residues for the best identified compounds of the phenolic acids and flavonoids (1-25) as identified by HPLC-MS extracts of *Thymelaea hirsuta* L., *Aloe vera* L., *Retama monosperma* L. and *Peganum harmala* L. with the targeted receptors: 1JIJ, 2QZW and 2UVO for TyrRS from *Staphylococcus aureus*, aspartic proteinase from *Candia albicans*, and wheat germ agglutinin, respectively.

Compound		Closest Interacting Residues	
No.	No. H-Bond	Residue (Letters & ID)	Distance to closest Interacting Residue (Å)
TyrRS from <i>Staphylococcus aureus</i> (pdb id: 1JIJ)			
12 (-10.5)	8	ASP40, LYS84, ARG88, ARG88, TYR170, HIS50, ASP40, ASP40, ASP195	LYS84:HZ1 (1.875)
11 (-9.9)	5	LYS84, LYS84, ASN124, ASP195, ASP177, LEU70	ASP177:OD1 (1.774)
10 (-9.7)	9	LYS84, LYS84, LYS84, LYS84, GLY193, GLN196, ASP195, THR75, GLY192, ASP40, ASP195, ALA39	LYS84:HZ2 (2.195)
Aspartic proteinase from <i>Candia albicans</i> (pdb id: 2QZW)			
8 (-10.0)	9	LYS49, SER89, ASN160, LYS178, SER336, GLY87, THR166, THR166, THR166, PRO4, ILE338	THR166:O (2.150)
7 (-9.9)	9	TYR81, TYR81, SER89, GLN168, SER336, SER334, SER88, THR6, GLY83, ILE338, GLY102;GLY103, PRO4, PRO4, PRO4	SER88:O (2.142)
10 (-9.9)	8	TYR225, SER301, SER301, SER334, GLY34, GLU193, SER301:HG ASP86, GLY220, ASP86, THR221, TYR225, ALA335	(2.173)
Wheat Germ Agglutinin (pdb id: 2UVO)			
16 (-8.4)	9	SER43, GLU72, TYR64, NDG1173, NAG1174, NDG1173, NAG1174, NDG1173, NAG1174, TYR64	NAG1174:O4 (1.890)
14 (-8.4)	5	TRP41, GLN59, CYS40, SER43, GLN59, NDG1173, NAG1174, NDG1173, NAG1174, GLU72	TRP41:O (1.817)
7 (-7.8)	5	SER43, TRP41, GLU72, NDG1173, NAG1174, NDG1173, NAG1174, NDG1173, NAG1174, TYR64	NAG1174:O4 (2.303)
Bold residues: interacting with Conventional H-Bonds			

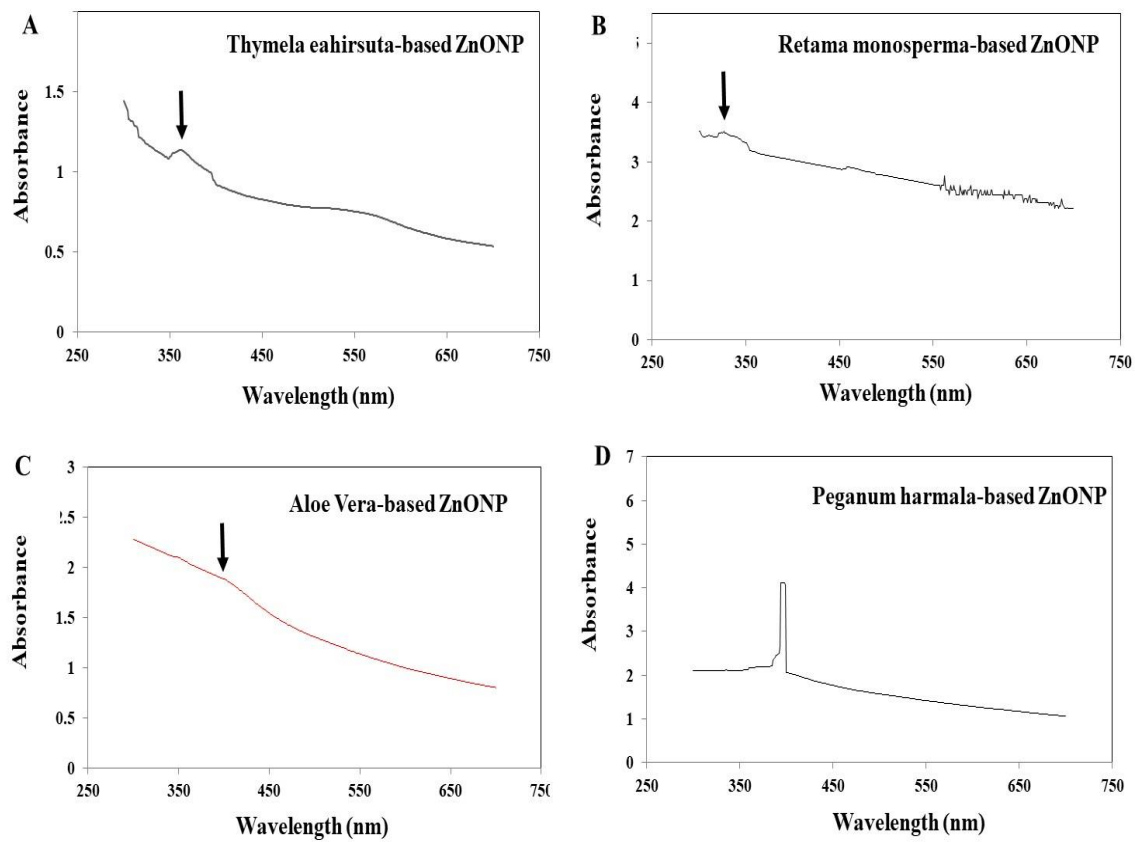
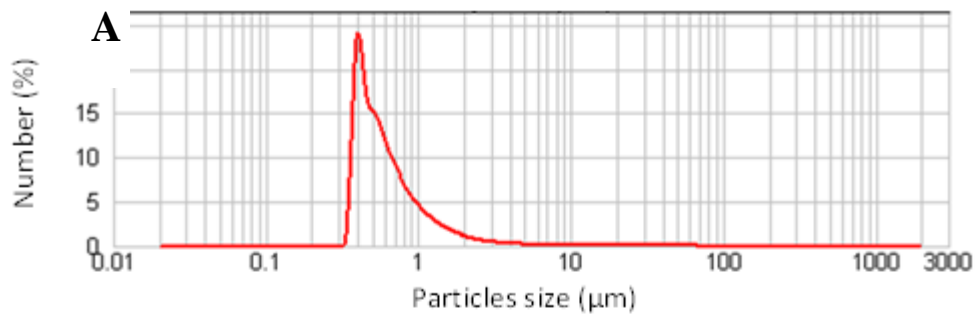
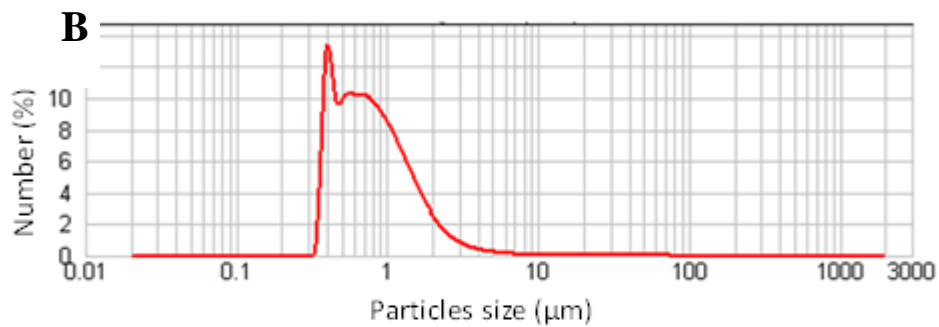


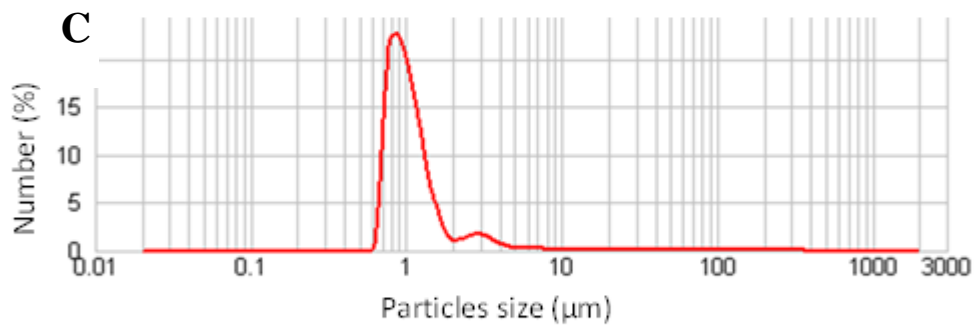
Figure 1. UV-Visible absorption spectrum of (A) *Thymhirs.* bio-ZnONP, (B) *Aloever.*bio-ZnONP, (C) *Retam.* bio-ZnONP and (D) *Harm.* bio-ZnONP.



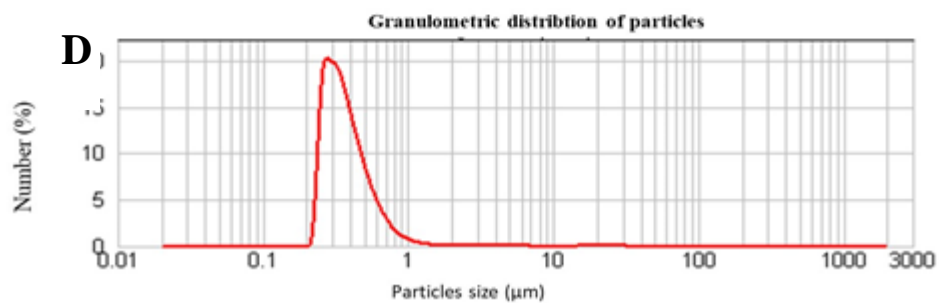
Thymelaea hirsuta L.



Aloe vera L.



Retama monosperma L.



Peganum harmala L.

Figure 2. Granulometry results of (A) *Thymhirs.* bio-ZnONP, (B) *Aloever.*bio-ZnONP, (C) *Retam.* bio-ZnONP and (D) *Harm.* bio-ZnONP.

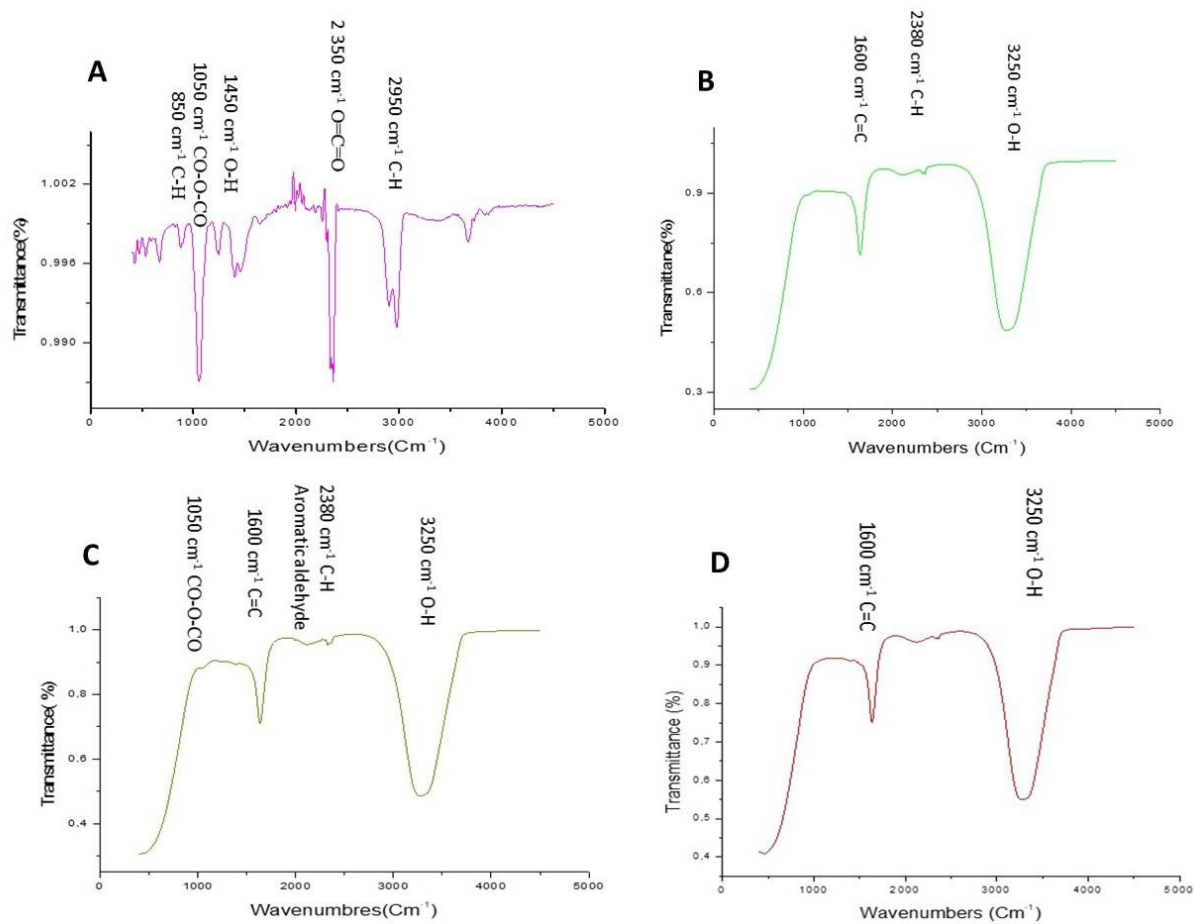


Figure 3. FTIR of (A) *Thymhirs.* bio-ZnONP, (B) *Aloever.* bio-ZnONP, (C) *Retam.* bio-ZnONP and (D) *Harm.* bio-ZnONP.

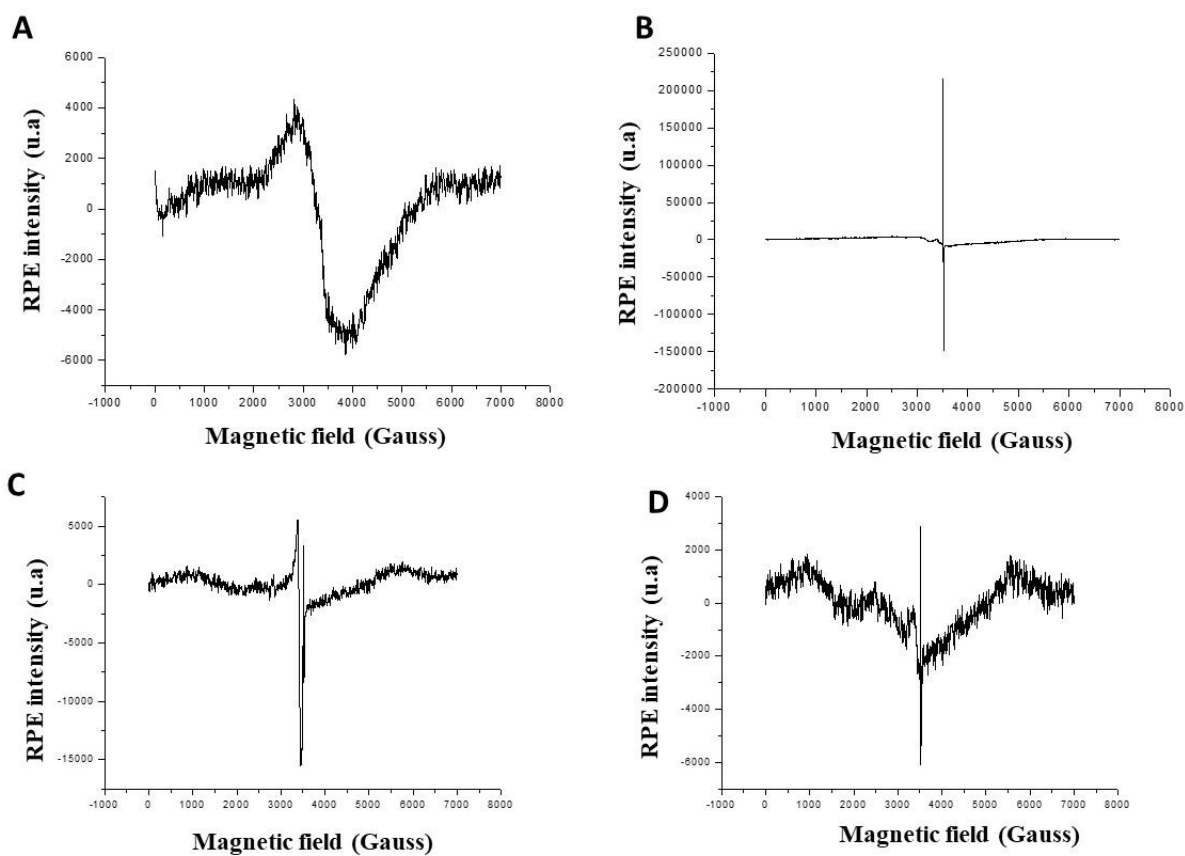


Figure 4. The electron paramagnetic resonance (EPR) spectra of (A) *Thymhirs.* bio-ZnONP, (B) *Aloever.* bio-ZnONP, (C) *Retam.* bio-ZnONP and (D) *Harm.* bio-ZnONP.

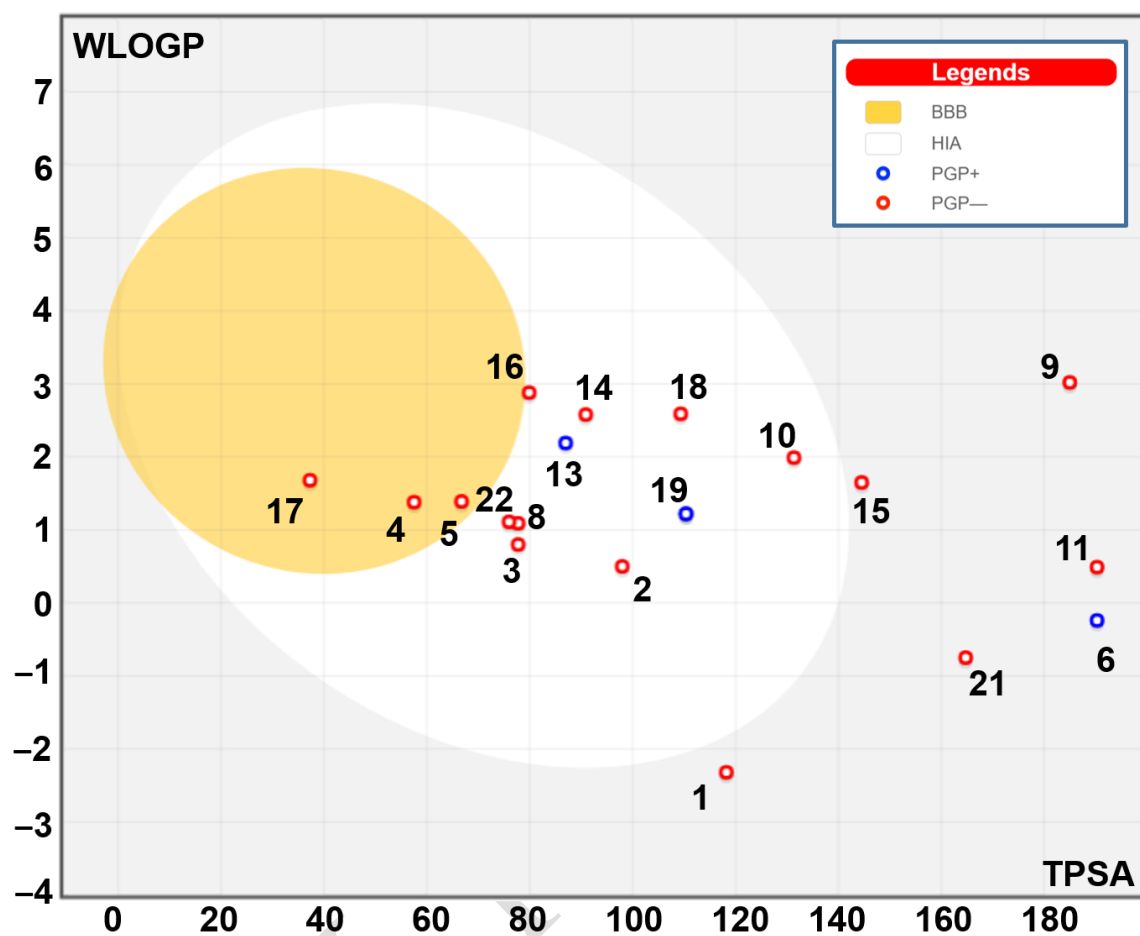


Figure 5. Boiled-egg model of the identified phytochemicals. The yellow and white areas correspond to the BBB permeation and GI absorption, respectively. Blue and red spots: phytochemical may or not be effluated by the P-glycoprotein.

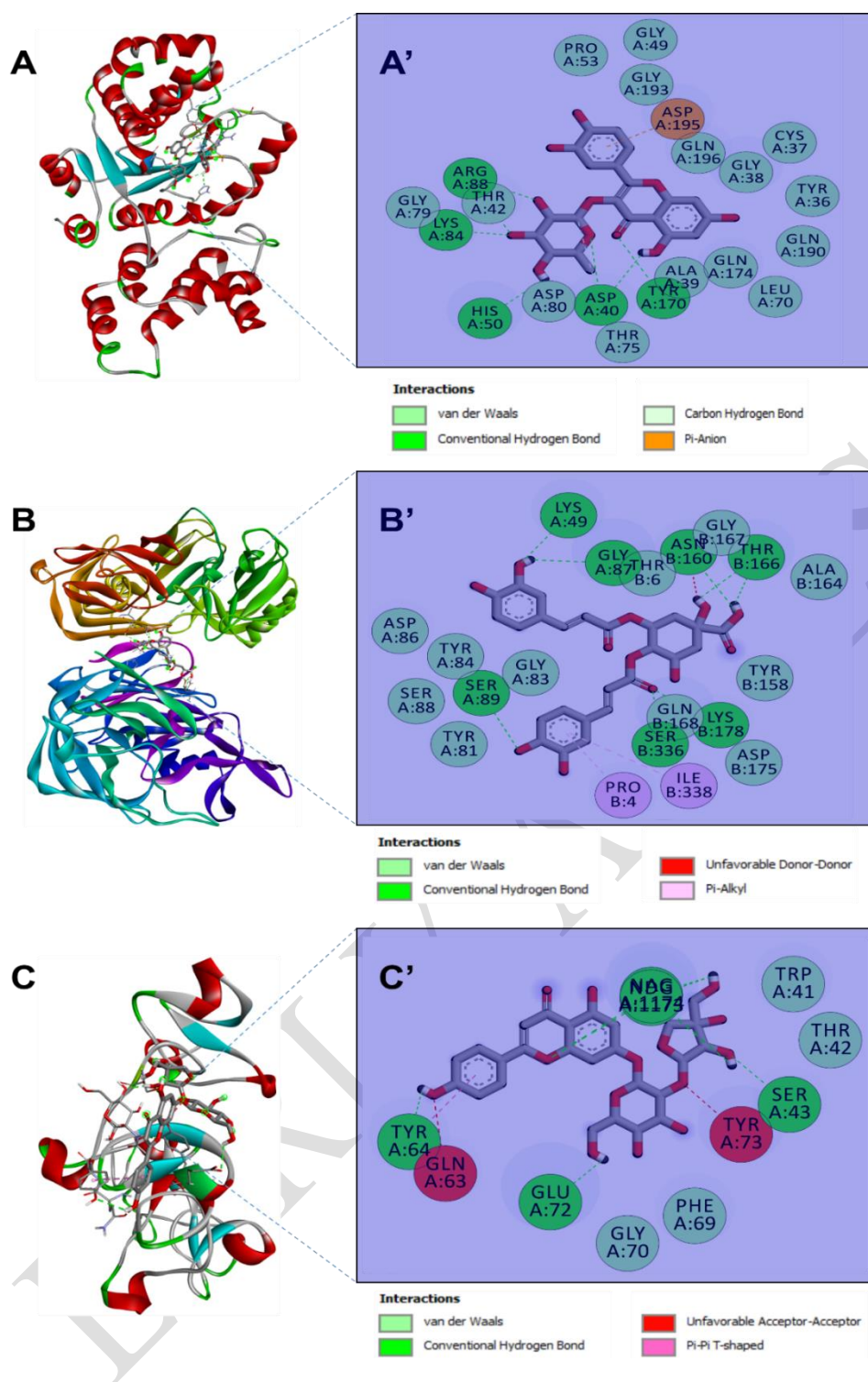


Figure 6. 3D views of the ribbon receptor–ligand complexes (A–C) and their corresponding 2D diagrams of interactions (A'–C') for the identified phytochemicals 12 (A and A'), 8 (B and B'), and 16 (C and C'), which have the best binding affinities (–10.5, –10.0, and –8.4 kcal/mol, respectively). The compounds are docked to 1JIJ (A and A'), 2QZW (B and B') and 2UVO (C and C').

SUPPLEMENTAL DATA

Supplementary data are available at the following link:

<https://www.bjms.org/ojs/index.php/bjms/article/view/12090/3883>

EARLY ACCESS